Quantitative analysis of reflection electron energy loss spectra to determine electronic and optical properties of Fe–Ni alloy thin films

Tahir, Dahlang; Oh, Suhk Kun; Kang, Hee Jae; Tougaard, Sven Mosbæk

Published in:
Journal of Electron Spectroscopy and Related Phenomena

Publication date:
2016

Document version
Final published version

Citation for pulished version (APA):
Tahir, D., Oh, S. K., Kang, H. J., & Tougaard, S. M. (2016). Quantitative analysis of reflection electron energy loss spectra to determine electronic and optical properties of Fe–Ni alloy thin films. Journal of Electron Spectroscopy and Related Phenomena, 206, 6-11.

Journal of Electron Spectroscopy and Related Phenomena 206 (2016) 6–11

Contents lists available at ScienceDirect

Journal of Electron Spectroscopy and Related Phenomena

journal homepage: www.elsevier.com/locate/elspec

Quantitative analysis of reflection electron energy loss spectra to determine electronic and optical properties of Fe–Ni alloy thin films

Dahlang Tahir[a,*], Sukh Kun Oh[b], Hee Jae Kang[b,**], Sven Tougaard[c,***]

[a] Department of Physics, Hasanuddin University, Makassar 90245, Indonesia
[b] Department of Physics, Chungbuk National University, Cheongju 362-763, Korea
[c] Department of Physics, Chemistry and Pharmacy, University of Southern Denmark, Odense M, Odense DK-5230, Denmark

ARTICLE INFO

Article history:
Received 27 June 2015
Received in revised form 8 September 2015
Accepted 6 November 2015
Available online 19 November 2015

Keywords:
Fe–Ni
REELS
ELF
Electronic properties
Optical properties

ABSTRACT

Electronic and optical properties of Fe–Ni alloy thin films grown on Si (1 0 0) by ion beam sputter deposition were studied via quantitative analyses of reflection electron energy loss spectra (REELS). The analysis was carried out by using the QUASES-XS-REELS and QUEELS-$\varepsilon(k,\omega)$-REELS softwares to determine the energy loss function (ELF) and the dielectric functions and optical properties by analyzing the experimental spectra. For Ni, the ELF shows peaks around 3.6, 7.5, 11.7, 20.5, 27.5, 67 and 78 eV. The peak positions of the ELF for $Fe_{28}Ni_{72}$ are similar to those of $Fe_{51}Ni_{49}$, even though there is a small peak shift from 18.5 eV for $Fe_{51}Ni_{49}$ to 18.7 eV for $Fe_{28}Ni_{72}$. A plot of n, k, ε_1, and ε_2 shows that the QUEELS-$\varepsilon(k,\omega)$-REELS software for analysis of REELS spectra is useful for the study of optical properties of transition metal alloys. For Fe–Ni alloy with high Ni concentration ($Fe_{28}Ni_{72}$), ε_1, and ε_2 have strong similarities with those of Fe. This indicates that the presence of Fe in the Fe–Ni alloy thin films has a strong effect.

1. Introduction

Quantitative surface analysis is one of the most efficient techniques for investigating surface-modification processes of technological importance, including surface oxidation and alloy formation. Electron-energy-loss spectroscopy (EELS) and reflection-electron-energy-loss spectroscopy (REELS) have previously been applied to quantitatively determine the inelastic electron-scattering cross section in solids [1–12]. In order to do that we need a clear understanding of the inelastic-scattering properties of electrons as they travel within the surface region of solids [1–9]. For this purpose two softwares, QUASES-XS-REELS [6] and QUEELS-$\varepsilon(k,\omega)$-REELS [4], were developed by Tougaard and Yubero [4]. The models adopted in these softwares also allow us to obtain the energy loss functions (ELF) and from this the dielectric as well as optical properties of a solid. The model has been tested experimentally and found to be in good agreement with REELS and XPS (X-ray photoelectron spectroscopy) experiments taken at different angles of incidence and emission [3,5,13]. The method has been applied to ultrathin dielectric films, semiconductors, metals and their oxides, transparent oxide films, and polymers [7,8,13–24].

The experimental inelastic cross section for electron-scattering was obtained from the measured REELS spectra by using the model described in Ref. [6] which has been implemented in the QUASES-XS-REELS software [1,2,6].

In the present work, we report on experimental inelastic-scattering cross section for electron-scattering of Ni and Fe–Ni alloys from REELS spectra for primary electron energies of 0.5, 1.0, 1.5 and 2.0 keV. We first use the QUASES-XS-REELS software to determine the effective inelastic-scattering cross section at each primary energy. Next we apply QUEELS-$\varepsilon(k,\omega)$-REELS software to determine the dielectric function which best describes these cross sections [1–5]. From this we also determine the electronic and the optical properties.

2. Experiments

Fe, Ni, and Fe–Ni alloy thin films were grown on silicon wafers by ion-beam sputter deposition (IBSD). The deposition chamber was connected to a surface analysis system, and thus the chemical state and composition of the deposited films could be analyzed in situ by XPS. The target material was sputtered by a 1 keV Ar^+ ion beam produced by a Kaufmann-type D.C. ion gun, and it was deposited on Si substrates at room temperature. The composition of the alloy thin films was controlled by varying the relative

* Corresponding author. Tel.: +62-411-586016.
** Corresponding author.
*** Corresponding author.
E-mail addresses: dtahir@fmipa.unhas.ac.id (D. Tahir), hjkang@cbu.ac.kr (H.J. Kang), svt@sdu.dk (S. Tougaard).

http://dx.doi.org/10.1016/j.elspec.2015.11.005
0368-2048/

sputtering areas of two adjacent target materials using a movable target holder. The films were grown on 150 mm diameter Si wafers, rotating with a speed of 30 rpm to assure thickness uniformity. The film thickness was controlled by selecting the growth time. The grown films had a physical thickness of ~200 nm and were cut into 10 mm × 10 mm specimens. Alloy thin film samples were prepared for a pilot study by the Surface Analysis Working Group of Consultant Committee for Amount of Substance (CCQM), and the compositions were certified by an isotope dilution method using inductively- coupled plasma-mass spectrometry. The alloy compositions in atomic % between Fe and Ni are 78%:22%, 51%:49%, and 28%:72%, respectively. The compositions measured with ex situ XPS, AES, and SIMS measurements under various experimental conditions agreed with the certified mean values to better than 2%. The Ar ion beam sputtering for removing contaminations did not change the composition nor induce sample in homogeneities on the Fe–Ni alloy sample surface since there is almost no mass difference between Fe and Ni. Details about the alloy composition of the Fe–Ni thin films can be found elsewhere [25]. In this experiment, 1 keV Ar ion beam sputtering was carried out for removing the contamination on the sample surface before the REELS measurement. REELS spectra of the samples were measured using an ESCAlab 210 instrument and recorded at a constant electron pass energy of 20 eV.

3. Data analysis

The first step in the analysis is to determine the effective experimental inelastic cross section from the REELS spectra with the QUASES-XS-REELS software [6]. This effective cross section $K_{exp}(\hbar\omega)$ includes surface and bulk excitations and as pointed out in the paper by Chorkendorff and Tougaard [6] it can contain small erroneous contributions from double surface and mixed surface and bulk excitations. These effects are however negligible (except for materials with a very narrow plasmon like Al [6]) since it has been found in numerous studies that these experimental cross sections are in good agreement with calculated theoretical single scattering cross sections of the surface and bulk contributions (see e.g., Refs. [7,8,13–24]).

For each REELS experiment the QUASES-XS-REELS software determines the experimental cross section $K_{exp}(\hbar\omega)$ times the corresponding inelastic mean free path λ, i.e., $\lambda K_{exp}(\hbar\omega)$.

3.1. Determination of energy loss functions (ELF)

As the second step in the analysis, the experimental cross sections are compared to theoretical cross sections $K_{th}(\hbar\omega)$ calculated with the QUEELS-$\varepsilon(k,\omega)$-REELS software. The input in these calculations is the ELF for which we use an expansion in Drude–Lindhard type oscillators [1–4];

$$Im\left\{\frac{-1}{\varepsilon(k,\omega)}\right\} = \theta\left(\hbar\omega - E_g\right) \bullet \sum_{i=1}^{n} \frac{A_i\gamma_i\hbar\omega}{\left(\hbar^2\omega_{0ik}^2 - \hbar^2\omega^2\right)^2 + \gamma_i^2\hbar^2\omega^2} \tag{1}$$

where the dispersion relation is given in the form

$$\hbar\omega_{0ik} = \hbar\omega_{0i} + \alpha_i\frac{\hbar^2k^2}{2m} \tag{2}$$

here $Im\left\{-1/\varepsilon(k,\omega)\right\}$ is the imaginary part of the reciprocal of the complex dielectric function. A_i, γ_i, $\hbar\omega$ and α_i are the oscillator strength, damping coefficient, excitation energy, and momentum–dispersion coefficient of the i_{th} oscillator, respectively, and $\hbar k$ is the momentum transferred by the inelastically scattered electron to the solid. The step function $\theta(\hbar\omega - E_g)$ is included to describe the effect of the band gap E_g in semiconductors and insulators. Here, $\theta(\hbar\omega - E_g) = 0$ if $\hbar\omega < E_g$ and $\theta(\hbar\omega - E_g) = 1$ if $\hbar\omega > E_g$. The value of α_i is related to the effective electron mass so that, in the present analysis, for oscillators corresponding to the valence electrons in metals we have used $\alpha_i = 1$ and for more tightly bound core electrons with flat energy bands $\alpha_i = 0.02$ [4,19]. The oscillator strengths in ELF are adjusted to make sure that $\varepsilon(k,\hbar\omega)$ fulfill the well-established Kramers–Kronig sum rule [2–4],

$$\frac{2}{\pi}\int_0^\infty Im\left\{\frac{1}{\varepsilon(\hbar\omega)}\right\}\frac{d(\hbar\omega)}{\hbar\omega} = 1 - \frac{1}{n^2} \tag{3}$$

where n is the refractive index in the static limit. For the Ni and Fe–Ni alloys we have used $1/n^2 \ll 1$. We used as the upper integration limit, the maximum energy loss in the experimental REELS and have thus ignored the small contribution from core electrons with larger binding energy. We note here that for higher energy loss λK_{exp} rapidly approaches zero.

The parameters in the ELF were determined by a trial and error procedure in which the parameters of a test ELF function are adjusted until there is good agreement between the theoretical $\lambda K_{th}(\hbar\omega)$ and experimental $\lambda K_{exp}(\hbar\omega)$ inelastic cross section for all primary energies considered.

3.2. Determination of optical quantities from ELF

From the ELF we can perform an analytical Kramers–Kronig transformation of $Im\{1/\varepsilon\}$ to obtain the real part $Re\{1/\varepsilon\}$ of the reciprocal of the complex dielectric function, [1,5]

$$Re\left[\frac{1}{\varepsilon(k,\hbar\omega)}\right] = 1 - \sum_{i=1}^{n}\frac{A_i\gamma_i\hbar\omega}{\left((\hbar\omega_{0ik})^2 - \hbar\omega\right)^2 + \gamma_i^2\hbar\omega^2}\cdot\theta\left(\hbar\omega - E_g\right) + \frac{2}{\pi}\int_0^{E_g} Im\left\{\frac{1}{\varepsilon(k,z)}\right\}\frac{zdz}{z^2-\omega^2} \tag{4}$$

From $Im\{1/\varepsilon\}$ and $Re\{1/\varepsilon\}$, the real and imaginary parts of the dielectric function ($\varepsilon = \varepsilon_1 - i\varepsilon_2$) and the refractive index N ($N = n - ik$, where n is the refractive index and k the extinction coefficient) are as follows,

$$\varepsilon_1 = \frac{Re\left\{1/\varepsilon\right\}}{\left(Re\left\{1/\varepsilon\right\}\right)^2 + \left(Im\left\{1/\varepsilon\right\}\right)^2} \quad \text{and}$$

$$\varepsilon_2 = \frac{Im\left\{1/\varepsilon\right\}}{\left(Re\left\{1/\varepsilon\right\}\right)^2 + \left(Im\left\{1/\varepsilon\right\}\right)^2} \tag{5}$$

$$n = \sqrt{\frac{1}{2}\left(\sqrt{\varepsilon_1^2+\varepsilon_2^2}+\varepsilon_1\right)} \quad \text{and} \quad k = \sqrt{\frac{1}{2}\left(\sqrt{\varepsilon_1^2+\varepsilon_2^2}-\varepsilon_1\right)} \tag{6}$$

Procedures to calculate these quantities from the ELF are included in the QUEELS-$\varepsilon(k,\omega)$-REELS software [4,5].

4. Results and discussion

Fig. 1 shows the comparison of the experimental inelastic-scattering cross section λK_{exp} (blue line) and theoretical inelastic cross section λK_{th} (red symbol line) for the studied Fe–Ni alloy thin films at primary electron energies of 0.5, 1.0, 1.5, and 2.0 keV. The ELF oscillator parameters used to calculate λK_{th} are listed in Table 1.

The parameters used to model the ELF and surface energy-loss function (SELF) for all materials considered are shown in Table 1. Those parameters should be done for the REELS taken at highest

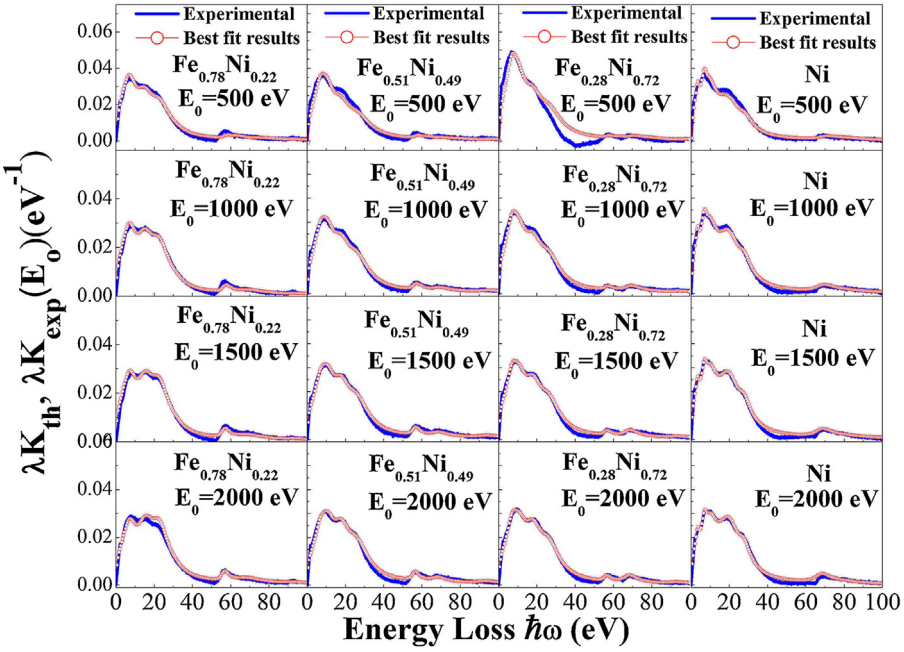

Fig. 1. Experimental inelastic cross section λK_{exp} for Fe–Ni alloys thin films (blue line) obtained from REELS data compared to theoretical inelastic cross sections λK_{th} (red symbol line) evaluated using the simulated energy-loss function given by the parameters in Table 1. (For interpretation of the references to color in this figure legend, the reader is referred to the web version of this article.)

Table 1
Parameters used to model energy-loss functions of Fe [19], Ni and Fe–Ni alloys using the model in [3] to give the best fit on the experimental cross section.

	i	$\alpha\omega_i$ (eV)	A_i (eV^2)	γ_i (eV)
Fe ($E_g = 0$) $\alpha_i = 1$ for $i \leq 4$) $\alpha_i = 0.02$ for $i \geq 5$) from Ref. [19])	1	9.4	13.2	8.0
	2	16.5	79.5	8.5
	3	23.6	261.6	10.0
	4	30.5	33.2	5.8
	5	56.0	24.2	2.7
	6	58.0	28.7	3.2
	7	66.8	138.0	16.0
	8	92	47.4	10.0
78% Fe ($E_g = 0$) $\alpha_i = 1$ for $i \leq 4$) $\alpha_i = 0.02$ for $i \geq 5$)	1	9.4	19.9	8.2
	2	16.5	79.7	8.5
	3	23.1	223.9	10.5
	4	30.5	10.2	6.0
	5	55.0	24.2	2.0
	6	56.5	28.3	2.0
	7	67.0	130.7	15.5
	8	91.0	43.5	10.0
51% Fe ($E_g = 0$) $\alpha_i = 1$ for $i \leq 4$) $\alpha_i = 0.02$ for $i \geq 5$)	1	8.4	5.4	6.5
	2	12.2	37.7	7.5
	3	18.5	116.6	9.5
	4	26.5	199.1	12.5
	5	55.5	55.4	3.0
	6	67.0	77.7	8.0
	7	91.0	89.6	10.0
28% Fe ($E_g = 0$) $\alpha_i = 1$ for $i \leq 4$) $\alpha_i = 0.02$ for $i \geq 5$)	1	8.4	6.0	6.0
	2	12.2	42.4	8.0
	3	18.7	118.6	9.5
	4	26.5	177.1	11.5
	5	55.5	32.2	3.0
	6	67.0	99.9	6.0
	7	91.0	45.4	8.0
Ni ($E_g = 0$) $\alpha_i = 1$ for $i \leq 5$) $\alpha_i = 0.02$ for $i \geq 6$)	1	3.6	0.4	2.1
	2	7.5	2.5	3.0
	3	11.7	36.9	8.0
	4	20.5	220.6	12.0
	5	27.5	68.2	6.5
	6	67.0	138.8	7.8
	7	78.0	42.8	15.0

energy and the same parameter also we apply for lowest energy. After examination of the difference between theoretical λK_{th} and experimental λK_{exp}, it is decided approximately what changes should be made by the trial dielectric function to improve agreement. We repeat several times to observed deviation between theoretical λK_{th} and experimental λK_{exp}. Finally, we decided those parameters after getting the best overall agreement between the theoretical λK_{th} and experimental λK_{exp} for all primary energies for each material was achieved. As seen in Fig. 1 good quantitative agreement between the theoretical inelastic cross section $\lambda K_{th}(E_0, \hbar\omega)$ and the experimental inelastic cross section $\lambda K_{exp}(E_0, \hbar\omega)$ was found for all alloys. The fact that the same ELF gives good agreement for all primary energies gives good confidence in the validity of the model and in the accuracy of the determined ELF's. There is only one exception to this good agreement namely for for $Fe_{78}Ni_{22}$ at 500 eV primary energy where the agreement is poor around 40 eV energy loss. This might be due to the effect mentioned above of the small difference in mixed surface and bulk excitations in the applied algorithm compared with the experimental situation [6]. This is however only expected when the plasmon loss is very narrow (like for Al [6]) and has not been an issue in numerous previous REELS analysis [7,8,13–24]. This small deviation was therefore ignored in the fitting procedure.

The ELF for pure Ni has 7 oscillators in the vicinity of 3.6, 7.5, 11.7, 20.5, 27.5, 67, and 78 eV. Comparison of the energy losses in the present results with previous reports [12,26,27] suggests that the energy loss peak at 7.5 eV is likely to be associated with the Ni 3d to Ni 4s transition or to a surface plasmon. This energy loss is similar to the oscillator for Pd at 8.0 eV [19] and Cu at 7.1 eV [15]. The stronger loss at 20.5 eV seems to be due to a bulk plasmon due to collective excitation of 4s and 3d electrons [16,17], which is also reported in Ref. [28]. The energy loss at 27.5 eV is attributed to an inter-band transition excitation of Ni 3d to 4s states [12,17]. The energy loss at 67 eV corresponds to the $M_{2,3}$ X-ray absorption edge [12].

The determined ELFs (Table 1) for Ni and the Fe–Ni alloys used as input parameters for the calculation of the theoretical cross-sections presented in Fig. 1 are depicted in Figs. 2 and 3. In Fig. 2,

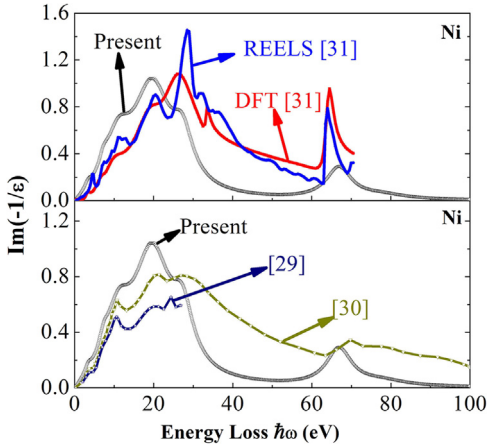

Fig. 2. Energy loss functions (ELF) for Ni in this study compared with results from Moravec et al. [29], Tokeshi et al. [30] and Werner et al. [31]. The strong deviations from Werner's result are explained in the text.

we compare our result for Ni to the ELFs published by Moravec et al. [29], Tokesi et al. [30], and Werner et al. [31]. Fig. 2 shows fair agreement with optical data for energy losses <30 eV, while it shows significant quantitative deviations for energy losses >30 eV. The optical data of Ref. [29] were limited to energy losses <30 eV and do not include excitations of Ni 3p and 3s electrons. Moravec et al. [29] determined the in ELF from a quantitative analysis of the optical conductivity, obtained from vacuum ultraviolet reflectometer, and interpreted in term of coherent potential approximation theory. Tokesi et al. [30], determined the ELF by a fit to the experimental optical data as compiled by Palik [32] using a sum of Drude functions and they are interpolate ELFs for other energies. The data of Werner et al. [31] in Fig. 2 were determined from an analysis of two REELS spectra obtained from well-characterized clean surfaces, measured at the primary electron energies E_0 = 700 eV and 3400 eV. The dielectric function is then determined by using a deconvolution model and convolutions of the surface and bulk terms for multiple scattering. A problem with this model was explained in Ref. [19]; the surface term is assumed to be independent of the primary energy and of the angle of electron trajectory to the surface normal, which is unlikely to be true [2,3,33]. The authors use a procedure (Eq. (27) in Ref.[31]) in which the statistical weight of the surface term only counts 1% and the bulk term counts 99% for the final fitting of the dielectric function. This subjective choice seems very strange. These authors also admit that the reason why they have to put such a small emphasis on the reliability of the surface term is due to inaccuracies in their model for the surface term [31].

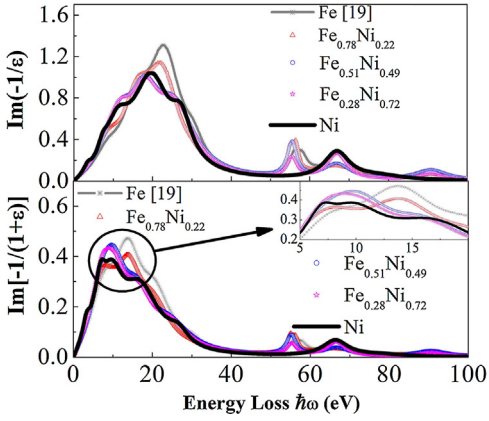

Fig. 3. Energy loss functions (ELF) and surface energy loss function (SELF) of Ni, Fe from Ref. [19] and the Fe–Ni alloys determined in this study.

Unfortunately thorough tests of the validity of Werner's model do not seem to have been done. For example, no tests have been published which show whether it provides consistent results when applied to sets of REELS spectra taken at various combinations of geometries and/or combination of the primary electron energies. However it was found [33] that inconsistencies resulted when the effective cross sections determined from REELS spectra from a wide range of energies were fitted by a linear combination of the surface and bulk energy-loss functions (which is an assumption applied in Werner's model). Moreover, it has been shown [2,3] that the shape of the energy loss distribution varies in a complex way both with the depth where the individual electrons in a REELS experiment are backscattered and with angle of emission [2,3]. These results all point to the conclusion that an analysis of REELS at low primary energies, expressed in terms of just two fixed functions, a bulk and a surface excitation function (as is assumed in [31]) is insufficient for a quantitative description. It is therefore not surprising that the model has deficiencies.

In contrast to this, the model that we have applied in this paper has been shown in numerous experimental examples to give a consistent dielectric function when applied to REELS taken with a wide range of energies and a wide range of geometries [7,8,13–24].

For these reasons, we ascribe the differences between the present results and those based on the REELS analysis in Ref. [31] to deficiencies in the applied model of Ref. [31].

We have no experience with the code and the model used for the density functional theory (DFT) calculations in Ref. [31] and can therefore not comment on the accuracy of these results.

For the Fe–Ni alloys (Fig. 3), we find peak positions that originate from the Ni and Fe in the alloy thin films. As can be seen in Table 1 and Fig. 3, all peak positions for the alloy come from combination of pure Fe [19] and Ni. For the alloy $Fe_{78}Ni_{22}$ with the highest concentration of Fe, the number of peaks is the same as that of pure Fe but several peaks are shifted to lower energy and have a reduced intensity. This is due to the decrease of Fe content and the corresponding change in electronic structure with increasing Ni content. The $Fe_{51}Ni_{49}$ alloy has 4 oscillators below 50 eV in the vicinity of 8.4, 12.2, 18.5, and 26.5 eV, which is somewhat different from those of both Fe and Ni. Energy losses at 67.0 eV and 55.5 eV comes from excitation of 3p electrons in pure Ni and pure Fe, respectively, which appeared as peaks at 56.0, 58.0, and 66.8 eV for Fe and 67.0 eV for Ni (see Table 1). The $Fe_{28}Ni_{72}$ alloy has 7 oscillators, which are very similar to those of $Fe_{51}Ni_{49}$, with only a small shift from 18.5 eV for $Fe_{51}Ni_{49}$ to 18.7 eV for $Fe_{28}Ni_{72}$ while the other peak positions are the same. We conclude that the electronic structure of $Fe_{51}Ni_{49}$ is very similar to that of $Fe_{28}Ni_{72}$.

The ELF's are dominated by a plasmon peak due to the excitation of the s and p valence electrons [12,13]. This is located at 23.6 eV for Fe [19] and moves gradually to lower energies in Fe–Ni alloys towards the bulk plasmon energy of Ni at 20.5 eV.

The strength of this oscillator also changes with the concentration of Fe and Ni. It is seen from Table 1, Figs. 2 and 3 that the strength decreases with decreasing amount of Fe in the alloy from 261.6 eV^2, 223.9 eV^2, 199.1 eV^2, and 177.1 eV^2 for Fe, $Fe_{0.78}Ni_{0.22}$, $Fe_{0.51}Ni_{0.49}$, and $Fe_{0.22}Ni_{0.78}$, respectively. We conclude that the number of electrons contributing to the collective excitations decrease with decreasing amount of Fe in the alloys [12].

Fig. 4 shows the real part ε_1 and the imaginary part ε_2 of the dielectric function for Ni (upper panels) and for the Fe–Ni alloys (lower panels). For Ni, the presently determined ε_1 and ε_2 are compared with the result of Werner et al. [31]. Large differences are evident. We ascribe these mainly to deficiencies in the model applied in Ref. [31] (see the detailed discussion above). Looking now at the lower panels, the highest peaks for the real

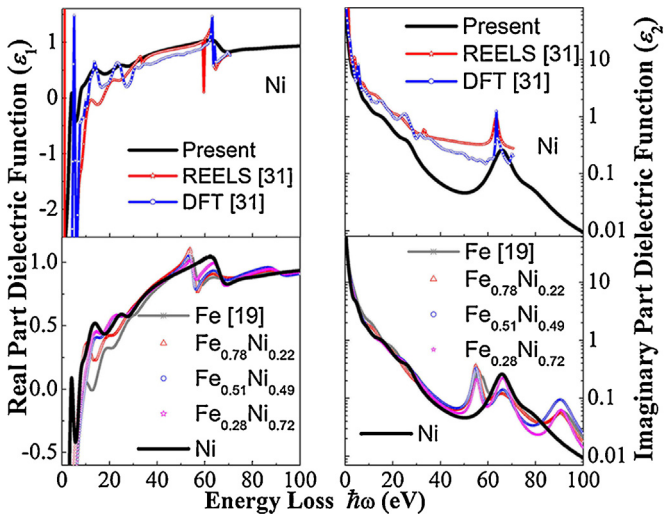

Fig. 4. Real part of the dielectric function (ε_1) and imaginary part of the dielectric functions (ε_2) of Ni and Fe–Ni alloys determined in this study as a function of energy. Also shown are the results obtained by Werner et al. for Ni via DFT calculations and his analysis of REELS taken at 700 eV and 3400 eV [31]. (For interpretation of the references to color in this figure legend, the reader is referred to the web version of this article.)

part of the dielectric function ε_1 are at 54.3, 51.91 eV, 53.47 eV, 53.57 eV, and 64.03 eV for Fe, $Fe_{0.78}Ni_{0.22}$, $Fe_{0.51}Ni_{0.49}$, $Fe_{0.22}Ni_{0.78}$, and Ni, respectively. For the imaginary part of the dielectric function ε_2, the highest peak are at 55.80, 53.74 eV, 54.93 eV, 55.16 eV, and 66.42 eV for Fe, $Fe_{0.78}Ni_{0.22}$, $Fe_{0.51}Ni_{0.49}$, $Fe_{0.22}Ni_{0.78}$, and Ni, respectively. The main peaks are shifted by 0.1–1.2 eV to higher energy-loss positions with decreasing Fe content in the alloy thin films from $Fe_{0.78}Ni_{0.22}$ to $Fe_{0.22}Ni_{0.78}$. This result indicates that the dielectric functions are not linearly dependent on Fe content in the Fe–Ni alloys. The dielectric function for Fe–Ni alloy thin films, even when the films contain 72% Ni, are closer to that of Fe rather than that for Ni. In the absorption spectrum, which is related to ε_2, the transparency of the Fe–Ni alloys and the Ni thin film for the energy-loss region above the bulk plasmon peak is higher than for the energy-loss region below the bulk plasmon peak [34,35]. This result is consistent with the fact that, in this energy-loss region (above the bulk plasmon peak), ε_2 and k go to zero as can be seen in Figs. 4 and 5.

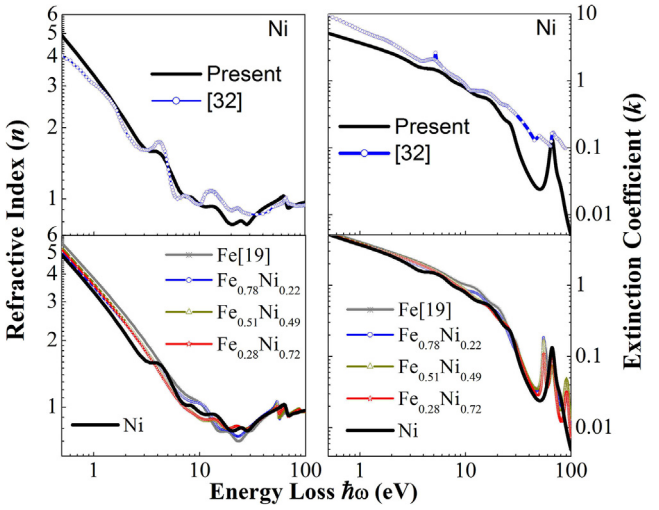

Fig. 5. Index of refraction (n) and extinction coefficient (k) of Ni and Fe–Ni alloys determined in this study as a function of energy. Also shown is the optical data for Ni compiled by Palik [32].

The upper panels in Fig. 5 show the refractive index n and extinction coefficient k as a function of energy loss for Ni (present work) together with corresponding data from Palik's handbook of optical data [32]. For Ni, Palik's compiled data are in reasonably good agreement with the presently determined n, while for k the agreement is good only for energy loss $\lesssim$20 eV. The origin of this is unknown. However, note that Palik took and compiled data from different publications. Note also that the data are ~35–45 years old and may be subject to experimental uncertainties caused, e.g., by surface contamination. The refractive index n and extinction coefficient k for the Fe–Ni alloys have magnitudes and peak positions that are different from those of pure Fe and pure Ni. From our results we conclude that the intensities, shapes, and peak positions of the dielectric function (ε_1 and ε_2), refractive index (n) and extinction coefficient (k) for Fe–Ni alloys are different from those of pure Fe and Ni even for an alloy with 72% Ni.

5. Conclusions

In this work, based on a model proposed by Tougaard and Yubero, a quantitative analysis has been made of REELS spectra obtained from Ni and Fe–Ni alloy thin films at primary electron energies of 0.5, 1.0, 1.5 and 2 keV. The ELFs for Ni and Fe–Ni alloy thin films were determined quantitatively by comparing the cross section for electron inelastic scattering from a theoretical calculation to that derived from experimental REELS spectra. The optical properties of Ni and Fe–Ni alloys have been determined from the ELFs and yielded good agreement with other results. The peak shapes and energy-loss positions of the ELF, ε_1, ε_2, n, and k indicate that the presence of Fe has a strong effect on the dielectric and optical properties of Fe–Ni alloy thin films even for an alloy with 72% Ni. The plot of ε_1, ε_2, n, and k show that REELS spectroscopy is a powerful method for the determination of optical properties of transition-metal alloys.

Acknowledgements

One of the authors (D. Tahir) would like thanks to the Hasanuddin University, Indonesia by BOPTN 2015 program for partial financial support of this research. This research was also partially supported by Basic Science Research Program through the National Research Foundation of Korea (NRF) funded by the Ministry of Education, Science and Technology (2012R1A1A2009590). S. Tougaard acknowledges the Danish Council for independent research (Natural Sciences) for financial support.

References

[1] S. Tougaard, J. Kraaer, Phys. Rev. B: Condens. Matter 43 (1991) 1651.
[2] F. Yubero, S. Tougaard, Phys. Rev. B: Condens. Matter 46 (1992) 2486.
[3] F. Yubero, J.M. Sanz, B. Ramskov, S. Tougaard, Phys. Rev. B: Condens. Matter 53 (1996) 9719.
[4] S. Tougaard, F. Yubero, QUEELS-$\varepsilon(k,\omega)$-REELS: Software Package for Quantitative Analysis of Electron Energy Loss Spectra; Dielectric Function Determined by Reflection Electron Energy Loss Spectroscopy. Version 3.0, 2008, See ⟨http://www.quases.com⟩.
[5] F. Yubero, S. Tougaard, Phys. Rev. B: Condens. Matter 71 (2005) 045414.
[6] S. Tougaard, I. Chorkendorff, Phys. Rev. B: Condens. Matter 35 (1987) 6570, Information about QUASES-XS-REELS software is available at ⟨http://www.quases.com⟩.
[7] H. Jin, S.K. Oh, H.J. Kang, S. Tougaard, J. Appl. Phys. 100 (2006) 083713.
[8] D. Tahir, E.K. Lee, S.K. Oh, H.J. Kang, S. Heo, J.G. Chung, J.C. Lee, S. Tougaard, J. Appl. Phys. 106 (2009) 084108.
[9] N. Pauly, S. Tougaard, F. Yubero, Phys. Rev. B: Condens. Matter 73 (2006) 035402.
[10] F. Yubero, L. Kover, W. Drube, Th. Eickhoff, S. Tougaard, Surf. Sci. 592 (2005) 1–7.
[11] D. Briggs, J.T. Grant, Surface Analysis by Auger and X-Ray Photoelectron Spectra, vol. 816, IM Publication, Manchester and Chichester, UK, 2003.
[12] H.A.E. Hagelin-Weaver, J.F. Weaver, Gar B. Hoflund, G.N. Salaita, J. Electron Spectrosc. Relat. Phenom. 134 (2004) 139.

[13] S. Hajati, O. Romanyuk, J. Zemek, S. Tougaard, Phys. Rev. B: Condens. Matter 77 (2008) 1.
[14] D. Tahir, S. Tougaard, J. Appl. Phys. 111 (2012) 054101.
[15] D. Tahir, S. Tougaard, J. Phys.: Condens. Matter 24 (2012) 175002.
[16] O. Romanyuk, P. Jiricek, J. Zemek, S. Tougaard, T. Paskova, J. Appl. Phys. 110 (2011) 043507.
[17] Y.S. Denny, H.C. Shin, S. Seo, S.K. Oh, H.J. Kang, D. Tahir, S. Heo, J.G. Chung, J.C. Lee, S. Tougaard, J. Electron Spectrosc. Relat. Phenom. 185 (2012) 18.
[18] H.C. Shin, D. Tahir, S. Seo, Y.R. Denny, S.K. Oh, H.J. Kang, S. Heo, J.G. Chung, J.C. Lee, S. Tougaard, Surf. Interface Anal. 44 (2012) 623.
[19] D. Tahir, J. Kraaer, S. Tougaard, J. Appl. Phys. 115 (2014) 243508.
[20] D. Tahir, Suarga, N.H. Sari, Yulianti, Appl. Rad. Isotopes 95 (2015) 59–62.
[21] D. Tahir, E.K. Lee, S.K. Oh, T.T. Tham, H.J. Kang, H. Jin, S. Heo, J.C. Park, J.G. Chung, J.C. Lee, Appl. Phys. Lett. 94 (2009) 212902.
[22] D. Tahir, E.K. Lee, E.H. Choi, S.K. Oh, H.J. Kang, S. Heo, J.G. Chung, J.C. Lee, S. Tougaard, J. Phys. D: Appl. Phys. 43 (2010) 255301.
[23] D. Tahir, Y.J. Cho, S.K. Oh, H.J. Kang, H. Jin, S. Heo, J.G. Park, J.C. Lee, S. Tougaard, Surf. Interface Anal. 42 (2010) 1566–1569.
[24] D. Tahir, E.K. Lee, S.K. Oh, H.J. Kang, E.H. Lee, J.G. Chung, J.C. Lee, S. Tougaard, Surf. Interface Anal. 42 (2010) 906–910.
[25] K.J. Kim, D.W. Moon, C.J. Park, D. Simons, G. Gillen, H. Jin, H.J. Kang, Surf. Interface Anal. 39 (2007) 665.
[26] A.P. Grosvenor, M.C. Biesinger, R.S.C. Smart, N.S. McIntyre, Surf. Sci. 600 (2006) 1771.
[27] E. Sickafus, F. Streinrisser, Phys. Rev. B: Condens. Matter 6 (1972) 3714.
[28] L.E. Koutsokeras, G.M. Matenoglou, P. Patsalas, Thin Solid Films 528 (2013) 49–52.
[29] T.J. Moravec, J.C. Rife, R.N. Dexter, Phys. Rev. B: Condens. Matter 13 (1976) 3297.
[30] K. Tokesi, L. Wirtz, C. Lemell, J. Burgdorfer, Phys. Rev. A: At. Mol. Opt. Phys. 64 (2001) 042902.
[31] W.S.M. Werner, K. Glantsching, C.A. Draxl, J. Phys. Chem. Ref. Data 38 (2009) 1013.
[32] E.D. Palik, Handbook of Optical Constants of Solids, Academic Press, New York, NY, 1985.
[33] F. Yubero, S. Tougaard, Surf. Interface Anal. 19 (1992) 269.
[34] L.K. Dash, N. Vast, P. Baranek, M.C. Cheynet, L. Reining, Phys. Rev. B: Condens. Matter 70 (2004) 245116.
[35] F. Wooten, Optical Properties of Solids, Academic Press, New York, NY, 1972.